# Dynamics of spiral waves rotating around an obstacle and the existence of a minimal obstacle

Xiang Gao,[1,2] Xia Feng,[3] Teng-Chao Li,[4] Shixian Qu,[1] Xingang Wang,[1] and Hong Zhang[4,*]

[1]*School of Physics and Information Technology, Shaanxi Normal University, Xi'an 710062, China*

[2]*Max Planck Institute for Dynamics and Self-Organization, Göttingen 37077, Germany*

[3]*Faculty of Science, Xi'an Shiyou University, Xi'an 710065, China*

[4]*Zhejiang Institute of Modern Physics and Department of Physics, Zhejiang University, Hangzhou 310027, China*

(Received 29 June 2016; published 30 May 2017)

Pinning of vortices by obstacles plays an important role in various systems. In the heart, anatomical reentry is created when a vortex, also known as the spiral wave, is pinned to an anatomical obstacle, leading to a class of physiologically very important arrhythmias. Previous analyses of its dynamics and instability provide fine estimates in some special circumstances, such as large obstacles or weak excitabilities. Here, to expand theoretical analyses to all circumstances, we propose a general theory whose results quantitatively agree with direct numerical simulations. In particular, when obstacles are small and pinned spiral waves are destabilized, an accurate explanation of the instability in two-dimensional media is provided by the usage of a mapping rule and dimension reduction. The implications of our results are to better understand the mechanism of arrhythmia and thus improve its early prevention.

DOI: 10.1103/PhysRevE.95.052218

## I. INTRODUCTION

Spiral waves, also known as vortices, are observed in chemical media [1–5] and biological systems [6–8] and also play a critical role in heart diseases [9–15], e.g., arrhythmia [16]. In this symptom, spirals tend to be pinned to inherent obstacles [17–21], such as complex anatomical structures, blood vessels, and even tissue damage [22]. Thus the rotation of a spiral wave around an obstacle is repeatedly found in both simulations [23–25] and experiments [26,27]. During these scenarios, spirals rotate around different-sized obstacles at corresponding periods. As obstacles shrink to some minimum, pinned spirals are destabilized and detached from obstacles [28,29]. Thus, theoretical analysis of their dynamics and instability is a fundamental question and has attracted much attention.

The kinematics of a spiral wave in a two-dimensional medium is much more complicated than the motion of an impulse in the one-dimensional case. One important reason for this is that the normal propagation velocity $C_n$ of the excited region boundary depends on the interface curvature $K$ as well as on the inhibitor value near the moving interface [30]. Tyson and Keener [31] adopted a linear form of the eikonal relation and got its approximate solution of the pinned spiral as their Eq. (22); however, the eikonal relation in the full parameter space is actually nonlinear. Adopting its linear form requires very small ratios of recovery rate to excitation rate $\epsilon$ [32] and very large periods of waves [33]. In Tyson and Keener's Eq. (22), any dependence of the rotation period of pinned spirals $T$ on the kinetics of models and excitability of the medium is through the dispersion relation for one-dimensional periodic waves; however, in applying the dispersion relation, they assumed a constant controller level along the wave front $v_f$. This assumption is valid only when the obstacle radius $r_0$ is large enough at the given excitability. However, the limitation of large $r_0$ is often violated in clinical treatment. For example, lidocaine is an antiarrhythmic agent commonly used to treat ventricular tachycardia. It lowers the excitability of heart, makes the obstacle not large enough at weaker excitability, and thus detaches the pinned spiral from the obstacle [34,35].

Hakim and Karma [36] also analyzed a solution to the linear eikonal relation of the pinned spiral in the weak excitability. They still assumed a constant $v_f$ that is only valid at large $r_0$. Recently, Loeber and Engel [37] proposed an improved theory compared to Tyson and Keener's, but they also adopted the linear eikonal relation and the constant $v_f$ assumption, which would limit their applications.

Despite so many theories attempting to study the dynamics of the spiral wave rotating around an obstacle, its instability is also broadly interesting. In other words, the question of common interest is how small an obstacle could be before the pinned spiral is destabilized and detached from it. The pioneers' theories have an instability inherited from the dispersion relation, since the rotation period of pinned spirals $T$ cannot be below a minimum where no periodic wave can exist [38], but they provide only acceptable estimates of the instability of pinned spirals. Another answer to this question is the concept of critical curvature [39–41]; however, as Refs. [39,41,42] stressed, this consideration provides a good estimate only in limited circumstances.

So far, the pioneers' theories to answer this fundamental question about the dynamics and instability of the pinned spiral have focused on some special circumstances such as large obstacles or weak excitabilities. Thus, a critical outstanding problem is a general theory that is also workable in many other interesting and important cases for both theoretical research and practical applications. In this paper we adopt a nonlinear form of eikonal relation [43], consider a variant $v_f$ along the wave front, and propose a general theory that is independent of special models. The theoretical results about the dynamics and instability fit the numerical simulation quantitatively, under all circumstances of obstacle sizes and excitabilities.

*Corresponding author: hongzhang@zju.edu.cn

 

## II. NUMERICAL SIMULATIONS

The dynamics and instability of the spiral wave rotating around an obstacle are studied in a two-component reaction diffusion system, with the FitzHugh-Nagumo model [44,45]. The FitzHugh-Nagumo model is a simplified version of the famous Hodgkin-Huxley model and a popular, generic, and dimensionless model also used by the pioneers' theories [36,37]. The equations used in our numerical simulations are

$$\frac{\partial u}{\partial t} = (3u - u^3 - v) + D\nabla^2 u, \tag{1}$$

$$\frac{\partial v}{\partial t} = \epsilon(u - \delta), \tag{2}$$

where $u$ and $v$ are the propagator and controller variables, respectively, and $D$ is the diffusion coefficient and chosen as unity without loss of generality. The excitability can be described by two parameters. One is $\epsilon$ [46]. The other is suggested to be $\Delta_0$ [47,48], which is equal to the difference between the controller levels at the stall value and at the rest state. In our chosen model, $\Delta_0$ is determined by the parameter $\delta$ as $\Delta_0 = \delta^3 - 3\delta$.

In the numerical simulations of Eqs. (1) and (2), we use the explicit Euler method and the finite-difference method in the polar coordinates. No-flux boundary conditions (BCs) are applied for the diffusion term of $u$ in Eq. (1) at both obstacle and medium boundaries. The initial condition to form a pinned spiral is by assigning the values of $u$ and $v$ of a plane wave onto the ring medium. Then this plane-wave initiation in the ring medium starts to propagate counterclockwise along the angular direction.

The radius of the obstacle starts from $r_0 = 80$. The radius of the ring medium is fixed at $R = 120$, which is large enough to avoid its effect on the dynamics and instability of pinned spirals. The spatial steps in the polar coordinates are $\Delta\rho = 0.1$ and $\Delta\theta = 2\pi/[2\pi(r_0 + R)/2\Delta\rho] \approx 9.9987 \times 10^{-4}$. Thus, in the radial direction, the grid number at the obstacle boundary is $N_1 = 800$ and the grid number at the ring medium boundary is $N_2 = 1200$. The total grid number along the radial direction is $N = N_2 - N_1 = 400$. Along the angular direction, the total grid number is $M = 2\pi/\Delta\theta = 6284$. The time step is $\Delta t = 0.0002$. After the plane-wave initiation and the transient process of the first three circulations of the pinned spiral, the rotation period $T$ for $r_0 = 80$ is measured as the average of periods for another three circulations.

To minimize the perturbation of the shrinking obstacle to the stability of the pinned spiral and to make sure that detachment is caused only by the small $r_0$ and not by the perturbation, a careful method of shrinking the obstacle is adopted as follows. The grid number at the obstacle boundary $N_1$ remains constant, while $\Delta\rho$ is multiplied by a scale factor 0.99. This would make the radius of the obstacle boundary shrink to be $r_0' = 0.99\Delta\rho N_1 = 0.99 r_0$. By keeping $N$, $M$, and $\Delta\theta$ constant, the values of $u$ and $v$ remain as the state of the pinned spiral; however, it is pinned to a smaller obstacle due to the nonuniform scaling. To avoid the effect of the ring medium boundary on the pinned spiral, its radius can be maintained at 120 by adding extra grids outside the original ring medium. The extra grids have $N' \times M$ points, where $N' = \lceil 120/(0.99\Delta\rho)\rceil - N_2$. The values of $u$ and $v$ in the extra grids can be assigned to be the rest state, without any disturbance on the critical obstacle boundary for the pinned spiral. According to the stability requirement, $\Delta t$ needs to be multiplied by $0.99^2$. Repeating the above shrinking method, one can get the accurate dynamics of pinned spirals at a geometric sequence of obstacle radius, until the instability of pinned spirals due to small $r_0$.

A weak excitability of $\epsilon = 0.013$ and $\Delta_0 = 0.704$ (i.e., $\delta = -1.60$) is chosen as our first example, since it is supposed to be also applicable to the pioneers' theories. In Fig. 1(a), a typical pattern in numerical simulations shows a spiral wave rotating counterclockwise around an obstacle of size $r_0$. The pinned spiral is near the instable point where the detachment happens, after a careful procedure of gradually shrinking $r_0$. To determine whether or not $v_f$ is constant, a natural coordinate $s$ along the wave front is established, as illustrated in Fig. 1(a) as a green directional dashed line. Then we check the value of $v_f$ from $s = 0$ to 220 above and find that $v_f$ changes nearly 10%. This proves that $v_f$ is not constant but varies when $r_0$ is small. From the numerical simulation results, we also confirm that the curvature $K$ at the obstacle boundary ($s = 0$) is the largest in the wave front and the normal velocity $C_n(s = 0)$ is slowest, as illustrated in Figs. 1(c) and 1(d) as the blue solid line.

To describe the dynamics of pinned spirals, one of the important profiles is the relationship between its rotation period $T$ and the obstacle radius $r_0$ [31,36,37]. In numerical simulations, we measure the accurate value of $T$ at dense data points of different $r_0$ and show it as the black solid line in Fig. 2. Note that the pinned spiral would be destabilized and detached from the obstacle when $r_0$ shrinks below 13.589.

## III. THEORETICAL ANALYSIS

To analyze theoretically the dynamics of the pinned spiral, we combine a nonlinear form of eikonal relation with kinematic equations as follow. The pinned spiral is governed by the eikonal relation, which describes the dependence of the normal velocity $C_n(s)$ on the curvature $K(s)$ for each segment on the wave front at the natural coordinate $s$. To remove limitations by its linear form and make it applicable to all circumstances of pinned spirals, we adopt a nonlinear form of eikonal relation [43] as

$$C_n(s) = C_p(T^\star(s), \epsilon^\star(s)) - DK(s), \tag{3}$$

where

$$T^\star(s) = T/[1 + DK(s)/C_p(T,\epsilon)], \tag{4}$$

$$\epsilon^\star(s) = \epsilon[1 + DK(s)/C_p(T,\epsilon)], \tag{5}$$

and $C_p(T,\epsilon)$ is the dispersion relation that gives the plane-wave velocity $C_p$ under given $T$ and $\epsilon$. Its value can be calculated by Winfree's method [46]. Although Eqs. (3)–(5) were derived for periodic target waves in Ref. [43], their applicability to a pinned spiral is confirmed by comparing their theoretical results with the numerical simulation results in Fig. 1(d). By substituting the rotation period $T$ and the curvature $K(s)$ obtained from the numerical simulations into Eqs. (3)–(5) and taking account of the known $\epsilon$ and the dispersion relation

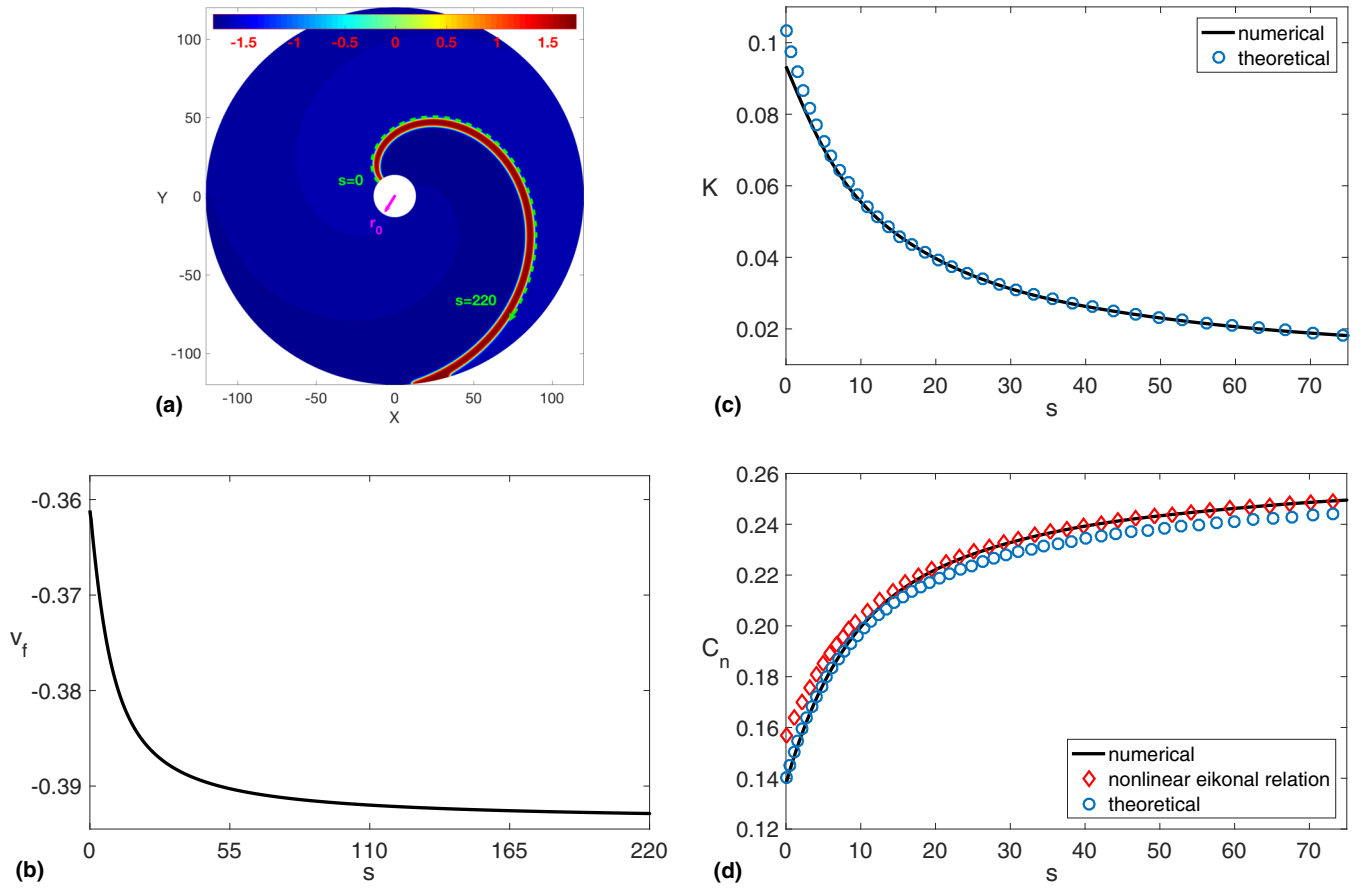


FIG. 1. (a) Spiral wave rotating counterclockwise around an obstacle in a disk-shaped excitable medium and bounded by no-flux boundary conditions at both the obstacle and medium boundary. Here the obstacle size $r_0 = 13.589$. In all simulations in this work, the medium size is large enough to neglect its effect. The green directional dashed line is the natural coordinate $s$ along the wave front. The wave front is defined as the contour of $u = 0$. (b) Variant $v_f$ along the natural coordinate $s$. (c) Numerical simulation and our theoretical results of curvature $K(s)$ along the natural coordinate $s$. (d) Normal velocity $C_n(s)$ along the natural coordinate $s$ obtained from the numerical simulation results of Fig. 1(a), the roots of the nonlinear eikonal relation by substituting the numerical results of $K(s)$ in (c) into Eqs. (3)–(5), and our theoretical results of Eqs. (3)–(7).

$C_p(T,\epsilon)$, the roots are the $C_n(s)$ given by the nonlinear eikonal relation, which are illustrated in Fig. 1(d) as open cyan diamonds. These roots only deviate slightly from the numerical simulation results near the obstacle boundary $s \to 0$ where the curvature $K(s)$ is large. The advantages of the nonlinear eikonal relation we adopt are no prerequisites of large $T$ and small $\epsilon$, the independence of any special models, and the applicability to all circumstances of excitabilities.

In addition, since the spiral wave is rigidly rotating around the obstacle, the wave front is sufficient to describe the entire pinned spiral alone. For each segment on the wave front at the natural coordinate $s$, its normal velocity $C_n(s)$, tangential velocity $C_\tau(s)$, and curvature $K(s)$ obey the kinematic equations [49,50]

$$\frac{dC_n(s)}{ds} = \frac{2\pi}{T} - K(s)C_\tau(s), \tag{6}$$

$$\frac{dC_\tau(s)}{ds} = K(s)C_n(s). \tag{7}$$

The deduction of these two equations is based on the kinematics of any rigidly rotating wave front [30]. Thus, they are model independent and applicable to all circumstances of pinned spirals.

The dynamics of the wave front is governed not only by Eqs. (3)–(7) but also by two no-flux BCs at both the obstacle and ring medium boundary. However, the ring medium boundary is large enough to avoid its effect on the dynamics and instability of pinned spirals. Thus, the no-flux BCs at the ring medium boundary could be replaced by the asymptotic solution of an unbounded spiral at $s \to \infty$ [30]. Thus, these equations are essentially a boundary-value problem.

To solve this boundary-value problem of Eqs. (3)–(7), we adapt a shooting method [51] as follow. With the given $r_0$ and $\epsilon$, we start with an arbitrarily chosen value of $C_n(0)$, hence $T = 2\pi r_0/C_n(0)$. Then we simultaneously solve Eqs. (3)–(5) at $s = 0$ to get $K(0)$. Since the central obstacle boundary is the no-flux BC, $C_\tau(0) = 0$. Taking the known $C_n(0)$, $C_\tau(0)$, and $K(0)$ as the initial conditions, we integrate Eqs. (6) and (7) along the wave front, at a sufficiently small integration step $\Delta s$, to get $C_n(\Delta s)$ and $C_\tau(\Delta s)$. Again, $K(\Delta s)$ is obtained by simultaneously solving Eqs. (3)–(5) as above. Moreover, at the given arc length $s$, the Cartesian coordinates $x(s)$ and $y(s)$ (whose origin is located at the center of the obstacle) and the

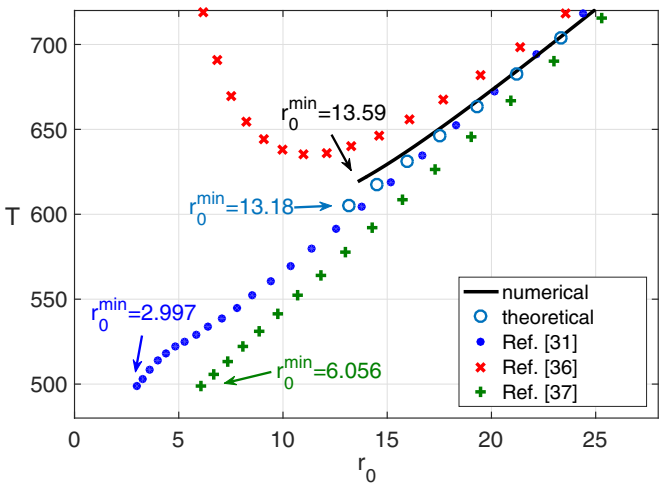


FIG. 2. Results of rotation periods of the pinned spiral $T$ at different obstacle sizes $r_0$ by numerical simulations, our theory, and pioneering theories by Tyson and Keener, Hakim and Karma, and Loeber and Engel. The $r_0 - T$ lines are cut off at different small $r_0$. These cutoff positions stand for the results about the instability of the pinned spiral where the detachment happens as $r_0$ reaches its minimal value $r_0^{\min}$. The excitability is $\epsilon = 0.013$ and $\Delta_0 = 0.704$ (i.e., $\delta = -1.60$).

angle $\theta(s)$ between the normal direction of the wave front and the $x$ axis are given by

$$x(s) = x(0) + \int_0^s \sin[\theta(s')]ds',$$
$$y(s) = y(0) - \int_0^s \cos[\theta(s')]ds',$$
$$\theta(s) = \theta(0) - \int_0^s K(s')ds',$$

where $x(0)$, $y(0)$, and $\theta(0)$ can be chosen arbitrarily [e.g., $x(0) = 0$, $y(0) = r_0$, and $\theta(0) = \pi$]. The polar coordinates $(r,\phi)$ can be written as $r(s) = \sqrt{x^2(s) + y^2(s)}$ and $\phi(s) = \arctan[y(s)/x(s)]$. Note that the periodic BC inherently in the polar coordinates implies the periodicity: $\phi = \phi + 2\pi$. Since we get $C_n(\Delta s)$, $C_\tau(\Delta s)$, and $K(\Delta s)$, the next integration may continue, until the ring medium boundary. As mentioned above, the no-flux BC at $r = R$ could be replaced as the asymptotic solution of an unbounded spiral for $s \to \infty$, which could be expressed as $C_n(s \to \infty) = C_p(T,\epsilon)$ and $C_\tau(s \to \infty) \to \infty$ since $K(s \to \infty) \to 0$. In this process, the initially guessed $C_n(0)$ would be rectified to its exact solution to meet these boundary conditions. This means that, using this shooting method, we can get $T$, $K(s)$, and $C_n(s)$ for all $s$ under the given $r_0$ and $\epsilon$. We illustrate the theoretical results of $K(s)$ and $C_n(s)$, respectively, in Figs. 1(c) and 1(d) as open cyan circles and demonstrate that they fit the numerical results well.

Hence, using this theory that is workable under all circumstances and independent of special models, we get the result of the $r_0 - T$ relationship as shown in Fig. 2 as the cyan open circles and find that it quantitatively fits the numerical simulation at any $r_0$. To compare with the pioneers' theories, we adapt their equations to the same format in this work based on the transformation rule made by Winfree [46]. Equation (22) in Tyson and Keener's Ref. [31] becomes

$$\frac{2\pi}{T} = \frac{C_p(4C_p r_0 + 1 - \sqrt{8C_p r_0 + 1})}{4r_0(C_p r_0 + 1)} \tag{8a}$$

when $r_0 > 0$. As for the case of $r_0 \approx 0$ and $C_p/\epsilon > 10$, it becomes

$$\frac{2\pi}{T} = m^* C_p^2 - \alpha^* C_p^4 r_0^2, \tag{8b}$$

where $m^* = 0.330958$ and $\alpha^* = 0.097$. Equation (44) in Hakim and Karma's Ref. [36] becomes

$$\frac{2\pi}{T} = \frac{C_p}{r_0} + \frac{2^{1/3} C_p^{1/3} a_1}{r_0^{5/3}}, \tag{9}$$

where $a_1 = -1.01879$. Equation (80) in Loeber and Engel's Ref. [37] becomes

$$\frac{2\pi}{T} = \frac{C_p^3(2\pi r_0 - TC_p)^2\sqrt{C_p^2(2\pi r_0 - TC_p)^2 - 16\pi^2}}{16\pi^2 r_0 C_p(2\pi r_0 - TC_p)\sqrt{\frac{r_0 C_p\sqrt{C_p^2(2\pi r_0 - TC_p)^2 - 16\pi^2}}{C_p(2\pi r_0 - TC_p)} + 1}}. \tag{10}$$

Within Eqs. (8)–(10), $C_p$ is also the dispersion relation $C_p(T,\epsilon)$. Thus, these equations are implicit functions of $T$, with $r_0$ and $\epsilon$ their variable and parameter, respectively. Their results of the $r_0 - T$ relationship are also shown in Fig. 2. Note that the pioneers' results deviate from the numerical simulation as $r_0$ shrinks.

The reason why our result maintains its accuracy at small $r_0$ while those of the pioneers do not is because our theory implicitly considers the fact that $v_f$ is not constant but varies. In Eq. (3), the dispersion relation is expressed as $C_p = C_p(T^\star(s),\epsilon^\star(s))$. It can also be expressed as $C_p(v_f)$ [52]. This means that $v_f$ can be viewed as a function of $s$ as $v_f = v_f(C_p) = v_f(T^\star(s),\epsilon^\star(s)) = v_f(s)$. In Eqs. (4) and (5), $T^\star(s)$ and $\epsilon^\star(s)$ depend on $K(s)$, and $K(s)$ varies with the natural coordinate $s$ along the wave front. Thus, $v_f$ would vary with $s$.

Besides the dynamics, our theoretical results about the instability of the pinned spiral also fit the results of simulation quantitatively, as shown in Fig. 2. The detailed analysis is presented as follow. The nonlinear eikonal relation in Eq. (3) needs the dispersion relation to evaluate the term $C_p(T^\star(s),\epsilon^\star(s))$. As shown in Fig. 3, the dispersion relation $C_p(T,\epsilon)$ obtained from Winfree's method [46] (gradient green surface) has an unstable boundary (red dashed line). Beyond this unstable boundary, no stable one-dimensional periodic wave exists at too small $T$ [38] or too large $\epsilon$ [46]. In our theory, shrinking the obstacle size $r_0$ makes $K(s)$ larger and thus makes $T^\star(s)$ in Eq. (4) smaller and $\epsilon^\star(s)$ in Eq. (5) larger. Finally, this drives $C_p(T^\star(s),\epsilon^\star(s))$ to approach the unstable boundary and includes its instability in the solution of the pinned spiral.

Furthermore, $K(s)$ at the obstacle boundary $s = 0$ is the largest along the wave front at given $r_0$, thus $T^\star(s = 0)$ is the smallest and $\epsilon^\star(s = 0)$ is the largest. This means that $C_p(T^\star(s),\epsilon^\star(s))$ at $s = 0$ is always the first to reach the unstable boundary of the dispersion relation. Therefore, we just need to consider its stability when $r_0$ shrinks. This is done by

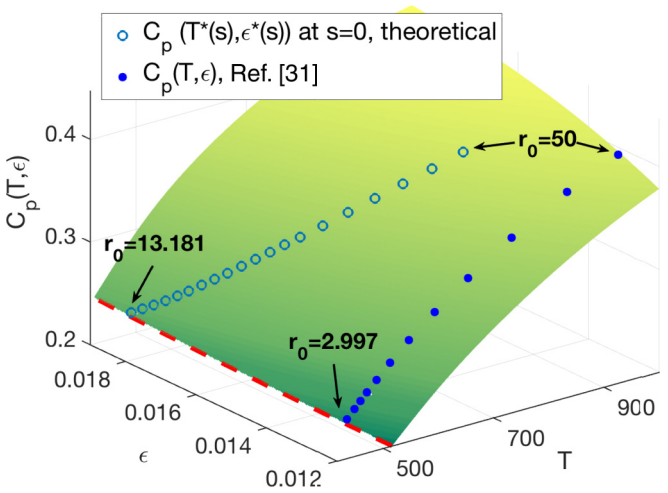


FIG. 3. Dispersion relation of $C_p(T,\epsilon)$ and its instability. The gradient green surface presents the dispersion relation in the concerned region. Its unstable boundary is highlighted by a red dashed line. The cyan open circles show how the term of $C_p(T^\star(s),\epsilon^\star(s))$ at $s = 0$ in our theoretical results approaches the unstable boundary as the obstacle size $r_0$ shrinks from 50 to 13.181. The blue closed circles indicate the destabilizing of $C_p(T,\epsilon)$ in Tyson and Keener's theory at the same excitability of $\epsilon = 0.013$ and $\Delta_0 = 0.704$ (i.e., $\delta = -1.60$) as $r_0$ shrinks from 50 to 2.997.

plotting the value of $C_p(T^\star(s = 0),\epsilon^\star(s = 0))$ for decreasing $r_0$ in Fig. 3 as the blue open circles, at the coordinates of $T = T^\star(s = 0)$ and $\epsilon = \epsilon^\star(s = 0)$. When the blue open circle of $C_p(T^\star(s = 0),\epsilon^\star(s = 0))$ reaches the red dashed line of the unstable boundary as $r_0$ shrinks, it just corresponds to the fact that in numerical simulations that the pinned spiral is detached from the obstacle boundary as the wave segment there becomes unstable and disappears.

In other words, the instability of the two-dimensional pinned spiral at given $T$ and $\epsilon$ is associated with the instability of the dispersion relation of one-dimensional periodic waves at $T^\star$ and $\epsilon^\star$, by a mapping rule defined in Eqs. (4) and (5). This can be viewed as a dimension reduction. However, the pioneers had no mapping rule. Taking Tyson and Keener's theory, for instance, shrinking $r_0$ gives a decreased $T$. By plotting their results of $C_p(T,\epsilon)$ in Fig. 3 at the coordinates of $T$ and $\epsilon$ as the blue closed circles, these circles would also reach the unstable boundary as $r_0$ shrinks. However, the values of $T$ and $\epsilon$ obtained for the instability of a two-dimensional pinned spiral are the same values as for an unstable one-dimensional periodic wave. This means that they borrowed the instability directly from one-dimensional periodic waves in two-dimensional pinned spirals without considering the difference between them. The same procedure applies to Loeber and Engel's theory, but Hakim and Karma's results diverge before meeting the unstable boundary of the dispersion relation. Thus, the results of [31,36,37] fail to anticipate a precise minimum $r_0$ before unpinning happens, as shown in Fig. 2.

To prove that our theory is valid at any excitability and obstacle size, we exemplify two other excitabilities, i.e., $\epsilon = 0.445$ and $\Delta_0 = 1.7429$ (i.e., $\delta = -1.28$) and $\epsilon = 0.013$ and $\Delta_0 = 1.9997$ (i.e., $\delta = -1.01$) as shown in Figs. 4(a) and 4(b), respectively. For both examples, our theoretical

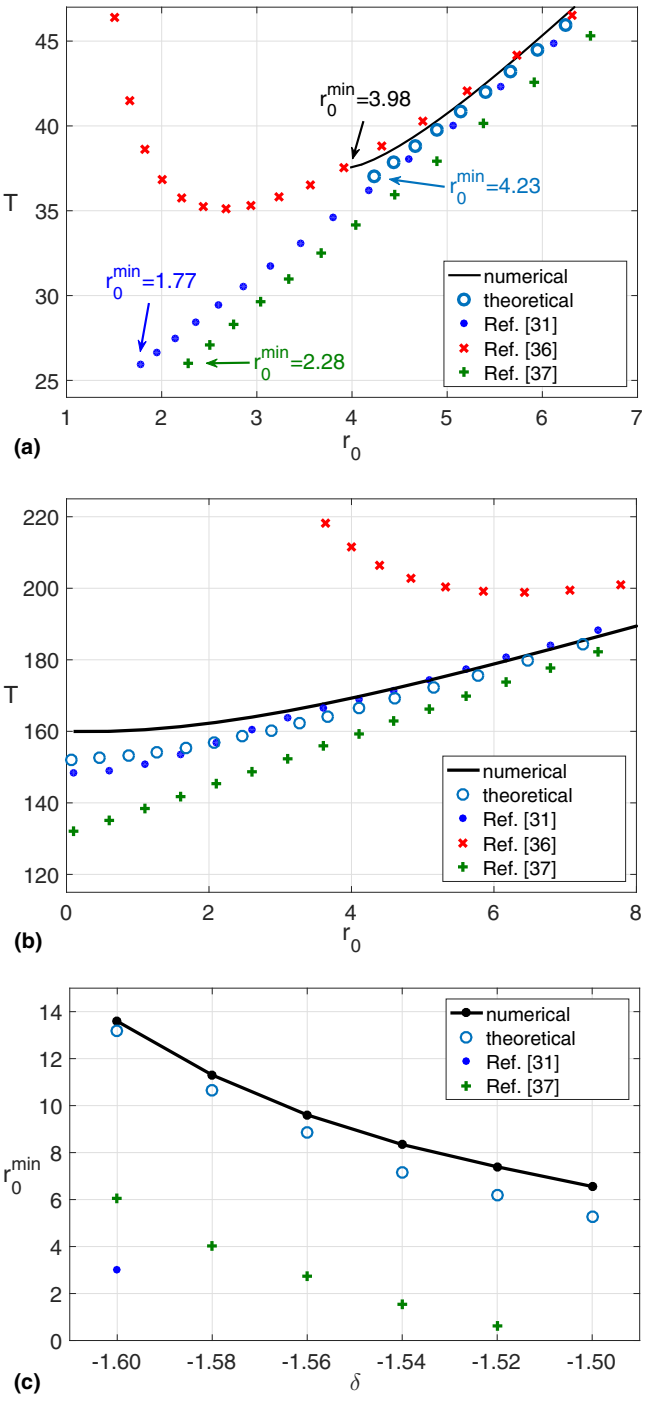


FIG. 4. Results of rotation periods of the pinned spiral $T$ at different obstacle sizes $r_0$ by the numerical simulations, our theory, and the pioneers' theories, at excitabilities of (a) $\epsilon = 0.445$ and $\Delta_0 = 1.7429$ (i.e., $\delta = -1.28$) and (b) $\epsilon = 0.013$ and $\Delta_0 = 1.9997$ (i.e., $\delta = -1.01$). (c) Comparison of minimal obstacle radius $r_0^{\min}$ results obtained by numerical simulations, our theory, and the pioneers' theories, at different excitabilities. The excitability is lowered by setting $\epsilon = 0.013$ and increasing $\delta$ from $-1.60$ to $-1.50$ in steps of 0.02.

results about the dynamics and instability also fit the numerical simulation quantitatively. Note that the second example is a high excitability, for which no detachment in numerical

simulations has been found at $r_0 \geqslant 0.01$. Further shrinking $r_0$ requires too much computational time. So far, we have demonstrated our theoretical results at three excitabilities and their corresponding various obstacle sizes. The three examples are randomly chosen from each corner of a trianglelike basin of spirals, as shown in Fig. 1 of Ref. [36]. The basin of spirals could also be the basin of pinned spirals, if sufficiently large obstacles are provided. Thus, the three examples demonstrate that our theoretical results about the dynamics and instability of pinned spirals fit numerical simulations in a reasonable random sampling from all circumstances.

Furthermore, Fig. 4(c) compares the results obtained by numerical simulations, our theory, and the pioneers' theories about the minimal obstacle radius $r_0^{\min}$ at different excitabilities. Numerical simulations show that $r_0^{\min}$ would decrease with decreasing excitability. Our theoretical results fit the numerical ones well. Loeber and Engel's method also reveals this tendency, but the deviations are large and it fails to identify $r_0^{\min}$ at $\delta = -1.50$. Tyson and Keener's method fails at $\delta \geqslant -1.58$ and Hakim and Karma's method fails in all cases.

## IV. DISCUSSION

It is worth mentioning that our theoretical results deviate slightly from numerical simulations when $r_0$ approaches the minimal obstacle radius $r_0^{\min}$. This is because smaller $r_0$ makes the curvature $K(s)$ larger. The nonlinear eikonal relation we adopt uses a finite renormalization technique and thus requires a relatively small curvature $K(s)$ [33,43]. However, as shown in Figs. 1(c), the curvature is no larger than 0.1 even when $r_0$ is nearly small enough to induce the detachment. This fact justifies the applicability of the nonlinear eikonal relation and thus our theory of the dynamics and instability of pinned spirals. In addition, our theory and the pioneers' theories just consider an isotropic excitable medium, which is common for theoretical analyses. For more complicated cases, such as the anisotropic medium [53], further investigation is needed.

## V. CONCLUSION

To summarize, we abandon the limitations of large obstacles or weak excitabilities adopted by the pioneers and propose a general theory for the dynamics and instability of pinned spirals. In particular, the destabilization is better understood by the implementation of a mapping rule and dimension reduction. This theoretical method to analyze the instability may shed light on other nonlinear problem. Our theoretical results quantitatively fit the numerical simulation under all circumstances. Finally, we emphasize that the FitzHugh-Nagumo model is too simple for simulating actual cardiac systems. In order to give useful instruction for practical applicability in real cardiac tissues, further investigation taking into account more realistic cardiac activities is needed.

## ACKNOWLEDGMENTS

This work was supported by the National Natural Science Foundation of China under Grants No. 11447026, No. 11675141, and No. 11647055 and by the Fundamental Research Funds for the Central Universities.

X.G. and X.F. contributed equally to this work.

[1] A. T. Winfree, Spiral waves of chemical activity, Science **175**, 634 (1972).

[2] K. I. Agladze and V. I. Krinsky, Multi-armed vortices in an active-chemical medium, Nature (London) **296**, 424 (1982).

[3] S. Jakubith, H. H. Rotermund, W. Engel, A. von Oertzen, and G. Ertl, Spatiotemporal Concentration Patterns in a Surface Reaction: Propagating and Standing Waves, Rotating Spirals, and Turbulence, Phys. Rev. Lett. **65**, 3013 (1990).

[4] Q. Ouyang and J. M. Flesselles, Transition from spirals to defect turbulence driven by a convective instability, Nature (London) **379**, 143 (1996).

[5] V. K. Vanag and I. R. Epstein, Inwardly rotating spiral waves in a reaction-diffusion system, Science **294**, 835 (2001).

[6] J. Lechleiter, S. Girard, E. Peralta, and D. Clapham, Spiral calcium wave-propagation and annihilation in xenopus-laevis oocytes, Science **252**, 123 (1991).

[7] S. Sawai, P. A. Thomason, and E. C. Cox, An autoregulatory circuit for long-range self-organization in Dictyostelium cell populations, Nature (London) **433**, 323 (2005).

[8] Y. Yu *et al.*, Reentrant spiral waves of spreading depression cause macular degeneration in hypoglycemic chicken retina, Proc. Natl. Acad. Sci. USA **109**, 2585 (2012).

[9] F. X. Witkowski *et al.*, Spatiotemporal evolution of ventricular fibrillation, Nature (London) **392**, 78 (1998).

[10] J. Jalife, Ventricular fibrillation: Mechanisms of initiation and maintenance, Annu. Rev. Physiol. **62**, 25 (2000).

[11] H. Zhang, Z. J. Cao, N.-J. Wu, H.-P. Ying, and G. Hu, Suppress Winfree Turbulence by Local Forcing Excitable Systems, Phys. Rev. Lett. **94**, 188301 (2005).

[12] S. Luther *et al.*, Low-energy control of electrical turbulence in the heart, Nature (London) **475**, 235 (2011).

[13] A. Karma, Physics of cardiac arrhythmogenesis, Annu. Rev. Condens. Matter Phys. **4**, 313 (2013).

[14] X. Feng, X. Gao, D.-B. Pan, B.-W. Li, and H. Zhang, Unpinning of rotating spiral waves in cardiac tissues by circularly polarized electric fields, Sci. Rep. **4**, 4831 (2014).

[15] Z. L. Qu, G. Hu, A. Garfinkel, and J. N. Weiss, Nonlinear and stochastic dynamics in the heart, Phys. Rep. **543**, 61 (2014).

[16] R. A. Gray, A. M. Pertsov, and J. Jalife, Spatial and temporal organization during cardiac fibrillation, Nature (London) **392**, 75 (1998).

[17] X. Q. Zou, H. Levine, and D. A. Kessler, Interaction between a drifting spiral and defects, Phys. Rev. E **47**, R800 (1993).

[18] O. Steinbock and S. C. Muller, Light-controlled anchoring of meandering spiral waves, Phys. Rev. E **47**, 1506 (1993).

[19] X. Wang, Y. Lu, M. Jiang, and Q. Ouyang, Attraction of spiral waves by localized inhomogeneities with small-world connections in excitable media, Phys. Rev. E **69**, 056223 (2004).

[20] D. Pazó, L. Kramer, A. Pumir, S. Kanani, I. Efimov, and V. Krinsky, Pinning Force in Active Media, Phys. Rev. Lett. **93**, 168303 (2004).
[21] V. N. Biktashev, D. Barkley, and I. V. Biktasheva, Orbital Motion of Spiral Waves in Excitable Media, Phys. Rev. Lett. **104**, 058302 (2010).
[22] E. M. Cherry and F. H. Fenton, Visualization of spiral and scroll waves in simulated and experimental cardiac tissue, New J. Phys. **10**, 125016 (2008).
[23] A. M. Pertsov, E. A. Ermakova, and A. V. Panfilov, Rotating spiral waves in a modified Fitz-Hugh-Nagumo model, Physica D **14**, 117 (1984).
[24] F. Xie, Z. L. Qu, and A. Garfinkel, Dynamics of reentry around a circular obstacle in cardiac tissue, Phys. Rev. E **58**, 6355 (1998).
[25] L. Glass, Y. Nagai, K. Hall, M. Talajic, and S. Nattel, Predicting the entrainment of reentrant cardiac waves using phase resetting curves, Phys. Rev. E **65**, 021908 (2002).
[26] J. M. Davidenko, A. V. Pertsov, R. Salomonsz, W. Baxter, and J. Jalife, Stationary and drifting spiral waves of excitation in isolated cardiac muscle, Nature (London) **355**, 349 (1992).
[27] M. Bar, N. Gottschalk, M. Eiswirth, and G. Ertl, Spiral waves in a surface reaction: Model calculations, J. Chem. Phys. **100**, 1202 (1994).
[28] A. V. Panfilov and J. P. Keener, Effects of high frequency stimulation on cardiac tissue with an inexcitable obstacle, J. Theor. Biol. **163**, 439 (1993).
[29] K. Agladze, J. P. Keener, S. C. Muller, and A. Panfilov, Rotating spiral waves created by geometry, Science **264**, 1746 (1994).
[30] V. S. Zykov, *Simulation of Wave Processes in Excitable Media* (Manchester University Press, Manchester, 1987).
[31] J. J. Tyson and J. P. Keener, Singular perturbation: Theory of traveling waves in excitable media, Physica D **32**, 327 (1988).
[32] J. P. Keener, A geometrical theory for spiral waves in excitable media, SIAM J. Appl. Math. **46**, 1039 (1986).
[33] A. M. Pertsov, M. Wellner, and J. Jalife, Eikonal Relation in Highly Dispersive Excitable Media, Phys. Rev. Lett. **78**, 2656 (1997).
[34] Z. Y. Lim, B. Maskara, F. Aguel, R. Emokpae, Jr., and L. Tung, Spiral wave attachment to millimeter-sized obstacles, Circulation **114**, 2113 (2006).
[35] A. Pumir, S. Sinha, S. Sridhar, M. Argentina, M. Hörning, S. Filippi, C. Cherubini, S. Luther, and V. Krinsky, Wave-train-induced termination of weakly anchored vortices in excitable media, Phys. Rev. E **81**, 010901 (2010).
[36] V. Hakim and A. Karma, Theory of spiral wave dynamics in weakly excitable media: Asymptotic reduction to a kinematic model and applications, Phys. Rev. E **60**, 5073 (1999). See the last paragraph of Sec. IV C 1.
[37] J. Loeber and H. Engel, Analytical approximations for spiral waves, Chaos **23**, 043135 (2013).
[38] J. Rinzel and J. B. Keller, Traveling wave solutions of a nerve conduction equation, Biophys. J. **13**, 1313 (1973).
[39] A. S. Mikhailov and V. S. Zykov, Kinematical theory of spiral waves in excitable media: Comparison with numerical simulations, Physica D **52**, 379 (1991).
[40] C. Cabo, A. M. Pertsov, J. M. Davidenko, and J. Jalife, Electrical turbulence as a result of the critical curvature for propagation in cardiac tissue, Chaos **8**, 116 (1998).
[41] V. Zykov, G. Bordyugov, H. Lentz, and H. Engel, Hysteresis phenomenon in the dynamics of spiral waves rotating around a hole, Physica D **239**, 797 (2010).
[42] E. Meron, Pattern formation in excitable media, Phys. Rep. **218**, 1 (1992).
[43] M. Wellner and A. M. Pertsov, Generalized eikonal equation in excitable media, Phys. Rev. E **55**, 7656 (1997).
[44] R. FitzHugh, Impulses and physiological states in theoretical models of nerve membrane, Biophys. J. **1**, 445 (1961).
[45] J. Nagumo, S. Arimoto, and S. Yoshizawa, An active pulse transmission line simulating nerve axon, Proc. IRE **50**, 2061 (1962).
[46] A. T. Winfree, Varieties of spiral wave behavior: An experimentalist's approach to the theory of excitable media, Chaos **1**, 303 (1991).
[47] A. Karma, Universal Limit of Spiral Wave Propagation in Excitable Media, Phys. Rev. Lett. **66**, 2274 (1991).
[48] V. S. Zykov, Kinematics of rigidly rotating spiral waves, Physica D **238**, 931 (2009).
[49] V. S. Zykov, N. Oikawa, and E. Bodenschatz, Selection of Spiral Waves in Excitable Media with a Phase Wave at the Wave Back, Phys. Rev. Lett. **107**, 254101 (2011).
[50] V. S. Zykov and E. Bodenschatz, Continuous Transition between Two Limits of Spiral Wave Dynamics in an Excitable Medium, Phys. Rev. Lett. **112**, 054101 (2014).
[51] X. Gao and H. Zhang, Mechanism of unpinning spirals by a series of stimuli, Phys. Rev. E **89**, 062928 (2014).
[52] J. P. Keener, Waves in excitable media, SIAM J. Appl. Math. **39**, 528 (1980).
[53] H. Dierckx, O. Bernus, and H. Verschelde, Accurate Eikonal-Curvature Relation for Wave Fronts in Locally Anisotropic Reaction-Diffusion Systems, Phys. Rev. Lett. **107**, 108101 (2011).